Charge trapping and scattering in epitaxial graphene

Damon B. Farmer,* Vasili Perebeinos, Yu-Ming Lin, Christos Dimitrakopoulos, and Phaedon Avouris
IBM T. J. Watson Research Center, Yorktown Heights, New York 10598, USA
(Received 29 August 2011; published 14 November 2011)

The Hall mobility and corresponding density of charge carriers in epitaxial graphene exhibit unexpectedly strong temperature dependence. This behavior is attributed to charge traps in the silicon carbide substrate that have a characteristic binding energy of approximately 70 meV. The electrostatic screening associated with these traps and the corresponding carrier transport behavior are investigated, as is transport at low densities, where the mobility sharply increases. The mobility at high carrier densities can be satisfactorily described by invoking Coulomb and short-range scattering. Scatterer transparency in the long-wavelength limit is suggested to occur in the low density regime, resulting in an abrupt mobility increase.

DOI: 10.1103/PhysRevB.84.205417 PACS number(s): 72.80.Vp, 72.20.Dp

I. INTRODUCTION

Electronic scattering by thermal excitations (phonons),[1,2] long-range interactions (charged impurities),[3–5] and short-range interactions (neutral defects)[6] can all manifest themselves in graphene.[7] The dominant scatterer depends on both the quality of the graphene and the characteristics of the environment in which the graphene exists. For instance, Coulomb scattering from charged impurities typically dominates at low temperatures when graphene is in contact with a substrate such as SiO_2 or Al_2O_3.[8,9] Due to the presence of absorbates, this is also the case when the substrate is removed and graphene is suspended. When graphene is heated and these absorbates are volatilized, phonon scattering becomes dominant, making high mobilities attainable.[10,11] However, if the graphene lattice is defective, scattering from neutral point defects dominates carrier transport.[12]

The type of scatterer that dominates transport in graphene can be revealed by the magnitude of the carrier mobility (μ) and its dependence on temperature (T) and carrier density (n). Mobilities greater than 100 000 cm^2/Vs are achieved when scattering is dominated by acoustic phonons, where $\mu_{AC} \propto 1/nT$.[8–11,13] Mobilities of this order can also be attained when surface polar phonons (SPP) dominate, where $\mu_{SPP} \propto 1/\sqrt{n}$.[8,13] Long-range, in-plane, Coulomb scattering results in mobilities on the order of 1000–10 000 cm^2/Vs that are independent of n.[3–5,14] In contrast, short-range, neutral defects reveal themselves either in highly defective samples or at high carrier densities, where $\mu_{SR} \propto 1/n$.[4,6,14] In light of these distinct dependences, the dominant scattering mechanism can cross over from one mechanism to another as n and/or T is changed.[8]

In this paper, we measure the Hall mobility and corresponding carrier density in epitaxially grown graphene[15,16] at different temperatures. We find an unexpectedly strong dependence of the density on temperature, which is ascribed to the trapping of carriers by charge traps in the SiC substrate.[17] Observation of this trapping effect has not been previously reported, and it gives insightful information about the material properties of epitaxially grown graphene. Previously unobserved transport behavior is also found to occur at very low carrier densities, where the mobility abruptly increases. Likely reasons for this behavior are also discussed.

II. EXPERIMENT

Top-gated graphene Hall bars are fabricated on single-layer graphene that was epitaxially grown on the silicon face of 6H(0001) SiC. The synthesis and characterization of this wafer-scale material are reported elsewhere.[18] With the aid of atomic force microscopy images of the sample surface, these Hall bars are oriented on topologically smooth areas and made relatively small: 3 μm between current probes, 1.5 μm between voltage probes (L), and 1 μm wide (W). The devices are then coated with a gate dielectric that consists of 10-nm NFC polymer and 20-nm HfO_2 and top gated with the same metal stack used for the source/drain electrodes (1-nm Ti/20-nm Pd/40-nm Au) [Fig. 1(a)]. Hall measurements of these devices are made in vacuum (10^{-8}–10^{-7} torr) at various temperatures (5–300 K). During these measurements, a constant current ($I = 10$ μA) is sourced between current probes, a magnetic field (B) is swept between -1 and 1 T to measure changes in the Hall voltage (V_y), and the gate is swept between $V_G = -8$ and 8 V to vary the Hall density ($n = IB/eV_y$). The resulting Hall mobility is then determined from the expression $\mu = V_y L / V_x BW$, where V_x is the Ohmic voltage between voltage probes.

III. HALL MOBILITY AND DENSITY

Figure 1(b) shows the measured mobility curves of a device at different temperatures as a function of the Hall density. As is typical of this material, the device is n-type with only the electron branch accessible within the gate voltage sweep range.[18] The small size of the Hall bar, coupled with the ability to orient it in a region that is topologically smooth, increases the probability of the device being located on an area with a high degree of electrostatic homogeneity, allowing for low densities to be achieved. Such is the case with this device, where Hall densities below 0.8×10^{12} cm^{-2} are attainable. Above this value, the Hall mobility steadily decreases with increasing density, as expected for single-layer graphene.[14] It is also apparent from these curves that, for the same gate voltage, higher temperatures allow higher Hall densities to be obtained. For instance, the 300 K curve extends to 4.8×10^{12} cm^{-2} at $V_G = 8$ V, while the 5 K curve only goes to 3.4×10^{12} cm^{-2}. In contrast to the gradual increase in the Hall mobility with decreasing density when $n > 0.8 \times 10^{12}$ cm^{-2}, the mobility

1098-0121/2011/84(20)/205417(5) ©2011 American Physical Society

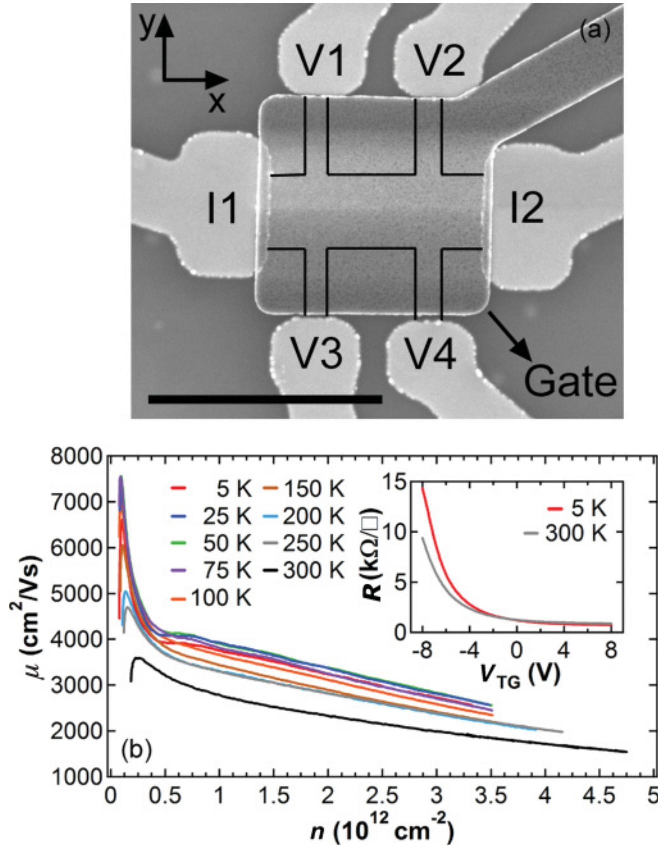

FIG. 1. (Color online) (a) Scanning electron microscopy image of the device showing the current probes (I1 and I2), voltage probes (V1–V4), and outline of the Hall bar underneath the gate (3-μm scale bar). (b) Hall mobility of the gated device as a function of Hall density at various temperatures. Inset: Resistance profile showing that the device exhibits n-type behavior.

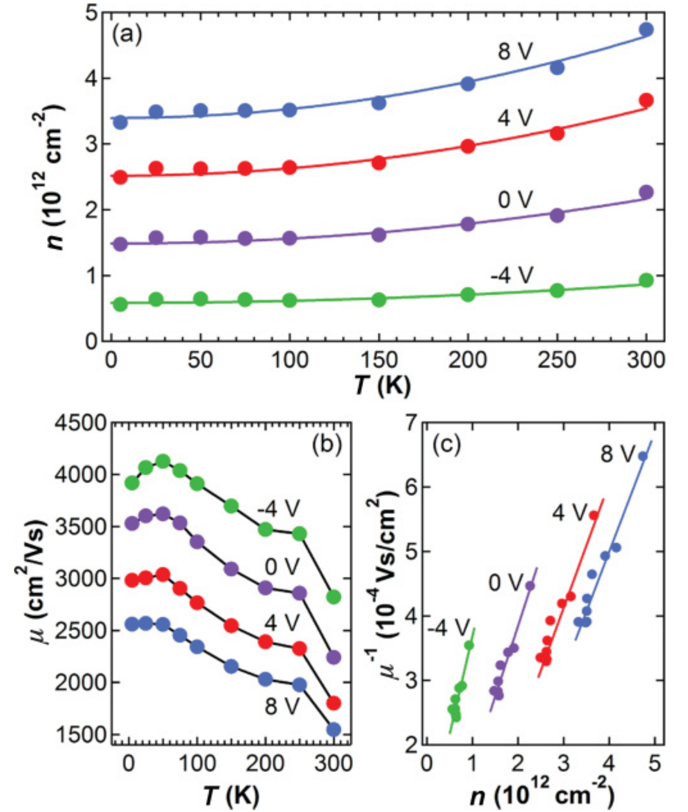

FIG. 2. (Color online) (a) Hall density at different gate voltages as a function of temperature (circles). With an activation energy of approximately 70 meV, the behavior of the density fits well to Eq. (1) (lines). At low temperature when $V_G = 0$, the intrinsic impurity density is found to be $n_i \approx 1.5 \times 10^{12}$ cm^{-2}. (b) The corresponding Hall mobility decreases with increasing temperature, and (c) its inverse is approximately linear with respect to the density.

rapidly increases when $n < 0.8 \times 10^{12}$ cm^{-2}. This increase becomes more pronounced at lower temperatures, where the highest mobility value of 7500 cm^2/Vs is obtained. Lower temperatures also enhance the on/off ratio of current traveling through the device, which is 11 at 300 K and 20 at 5 K [Fig. 1(b) inset].

A. High density regime: charge traps

The temperature dependence of the maximum attainable carrier density is the most striking feature of the data presented in Fig. 1(b) and is the central result of this paper. This behavior can be described by the general expression

$$n = n_{T=0}(1 + Be^{-E_a/k_BT}), \tag{1}$$

where E_a is an activation energy, B is a global fitting parameter, and $n_{T=0}$ is the Hall density at zero temperature. Equation (1) is plotted with the experimental data as a function of temperature at different gate voltages in Fig. 2(a). The Arrhenius-type behavior shown here indicates that transport in the $n > 0.8 \times 10^{12}$ cm^{-2} regime is heavily influenced by carrier activation with an activation energy of $E_a \approx 70$ meV. The corresponding temperature dependence of the Hall mobility is presented in Fig. 2(b), where it is shown to decrease nonlinearly with increasing temperature. Since the buffered dielectric used in this experiment causes carrier mobility in graphene to exhibit a distinctly different temperature dependence,[19] it is reasonable to conclude that the observed behavior is associated with the SiC substrate.

In principle, the modulation of Hall density and mobility with temperature can be caused by several scattering mechanisms. This observation in epitaxial graphene has been previously attributed to the interaction of carriers with SPP phonons.[20] However, the magnitudes of the mobilities reported here and in Ref. 20 are too low to be SPP limited.[13] The 40% decrease in mobility [Fig. 2(b)] also cannot be accounted for by acoustic phonons[8] or the temperature dependence of Coulomb scattering,[21] and optical phonons do not significantly couple to carriers with energies below 200 meV.[22,23] Furthermore, the 40% increase in density [Fig. 2(a)] is not due to thermal excitation of carriers (specifically minority carriers) at high density, which is determined by analysis of Eqs. (3) and (8) outlined later. For these reasons, we suggest that charge traps are the most likely cause of the observed temperature dependence.

To better understand the physics underlying this behavior, the measured data are analyzed using Boltzmann transport theory. In this model, the carrier mobility limited by Coulomb

impurity scattering (e.g., scattering from charge traps) takes the form

$$\mu_C(T,n_{\text{tot}},d) = \frac{ev_F^2}{2n_{\text{tot}}}\sum_{s=\pm1}\int_0^\infty D(E)\tau_C(E,E_F,T,d) \times \left(-\frac{\partial f_s(E,E_F,T)}{\partial(sE)}\right)dE, \quad (2)$$

where $D(E) = 2E/\pi\hbar^2 v_F^2$ is the density of states, v_F is the Fermi velocity at the Fermi energy (E_F), $f_s(E,E_F,T) = (\exp[(sE - E_F)/k_BT] + 1)^{-1}$ is the Fermi-Dirac distribution function, $\tau_C(E,E_F,T,d)$ is the scattering time, $s = +1$ (-1) for electrons (holes), and

$$n_{\text{tot}}(E_F) = n_e + n_h = \int_0^\infty D(E)(f_{+1}(E,E_F,T)+1-f_{-1}(E,E_F,T))\,dE \quad (3)$$

is the sum of the electron (n_e) and hole (n_h) carrier densities. In the unipolar regime, where $n \gg k_B^2T^2/\pi\hbar^2v_F^2$ and $n \gg n_{pd}$, with n_{pd} being the electron/hole puddle density associated with the graphene surface,[25] the measured Hall density is equal to this sum ($n = n_{\text{tot}}$). The scattering rate associated with Coulomb scattering is given by[24]

$$\frac{1}{\tau_C(E,E_F,T,d)} = \frac{\pi n_i}{\hbar}\int\frac{1}{(2\pi)^2}\left|\frac{V(q,d)}{\varepsilon(q,T,E_F)}\right|^2 \times (1-\cos^2\theta)\delta(E_k - E_{k'})d^2k', \quad (4)$$

where $q = |k - k'| = 2k|\sin(\theta/2)|$, d is the perpendicular distance of the scatterer from the graphene plane, n_i is the scatterer (impurity) concentration, θ is the scattering angle, and $\varepsilon(q,T,E_F)$ is the dielectric screening function.[21] For Coulomb scattering, $V(q,d) = (2\pi e^2/\kappa q)e^{-qd}$, where κ is the average dielectric constant of the environment around the scattering centers.[4] The scattering rate is evaluated using the random phase approximation (RPA),[21] allowing for determination of μ_C and comparison to the data.

Such a comparison is made by determining the change in the Coulomb-limited mobility as the impurity density changes with temperature due to thermalization of the charge traps, i.e., evaluating $d\mu_C^{-1}/dn_i$ from the experimental data. This differential is put in terms of measurable quantities ($d\mu^{-1}/dn$) by first recognizing that the total carrier density can be expressed as $n_e - n_h = n_i + (C_GV_G/e)$, where C_GV_G/e is the charge density induced by the gate electrode at a voltage V_G with capacitance C_G. At the charge neutrality point V_{NP}, $n_e - n_h = 0$ and $V_G = V_{\text{NP}}$, which stipulates that $C_GV_{\text{NP}}/e = -n_i$. The traps can therefore be considered to be positive since V_{NP} is negative and the Hall density increases with increasing temperature [Figs. 1(b) inset and 2(a)]. Far from the neutrality point, in the unipolar, high density regime, $n_h = 0$ and $n = n_e$. Measuring the change in the Hall density (dn) with temperature at constant V_G therefore allows the change in the trapped charge density (dn_i) to be determined ($dn = dn_i$). The temperature evolution of the inverse Hall mobility at high densities exhibits a linear density dependence [Fig. 2(c)], which can be described in terms of short-range and Coulomb scattering using Matthiessen's rule $\mu^{-1} = \mu_C^{-1} + \mu_{\text{SR}}^{-1} = \mu_C^{-1} + A_{\text{SR}}n$, where A_{SR} is a scaling

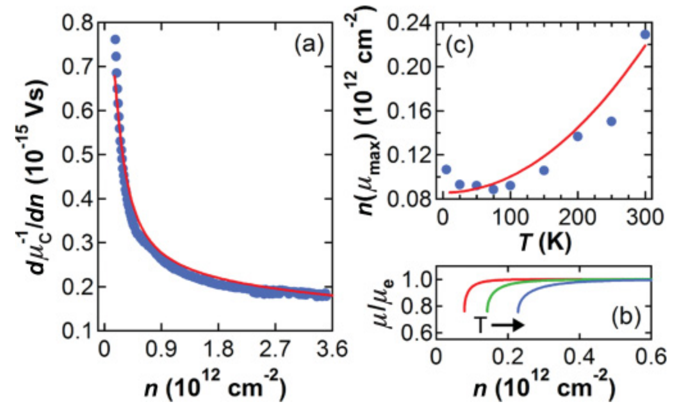

FIG. 3. (Color online) (a) Experimental values of $d\mu_C^{-1}/dn$ (blue [light gray] circles) and the corresponding calculated values, assuming Coulomb scattering from the charge traps according to Eqs. (2) and (6) using RPA formalism for $d = 0.5$ nm, $\kappa = 3.3$, and $T = 300$ K (red [dark gray] curve). (b) Calculated values of the ratio of Hall mobility to electron mobility at different temperatures assuming two-carrier transport: 50 K (red [left]), 200 K (green [middle]), and 300 K (blue [right]). Here, symmetric electron and hole mobility is assumed ($\mu_e = \mu_h$). (c) Hall density at the rollover point as a function of temperature (blue [light gray] circles). The behavior is described well using Eqs. (7) and (8) and a value of $n_{pd} \approx 4.7 \times 10^{10}$ cm^{-2}, as outlined in the main text (red [dark gray] curve).

factor for the short-range potential. Differentiating with respect to the Hall density leads to the final expression

$$\frac{d\mu_C^{-1}}{dn_i} = \frac{d\mu_C^{-1}}{dn} = \frac{d\mu^{-1}}{dn} - A_{\text{SR}}, \quad (5)$$

where A_{SR} is determined in the analysis presented in Sec. III C. Using Eq. (5), the experimental data may now be compared to the theoretical prediction, which is computed from the relation

$$\frac{d\mu_C^{-1}}{dn_i} = \frac{\partial\mu_C^{-1}}{\partial n_i} + \frac{dn_{\text{tot}}}{dn_i}\frac{\partial\mu_C^{-1}}{\partial n_{\text{tot}}} = (n_i\mu_C)^{-1} + n_i\frac{\partial}{\partial n_{\text{tot}}}(n_i\mu_C)^{-1}, \quad (6)$$

where μ_C is calculated using Eqs. (2)–(4). The second term in Eq. (6) arises from both n_i and n_{tot} being modified with temperature such that $dn_i = dn_{\text{tot}}$ in the unipolar regime. A summary of this analysis is presented in Fig. 3(a), where good agreement between the experimental and the theoretical derivatives is attained at high densities using a reasonable choice of $d = 0.5$ nm and $\kappa = 3.3$ in the calculation. Here, a value of $n_i = 1.5 \times 10^{12}$ cm^{-2} is used in Eq. (6), which is based on the intrinsic impurity density ($V_G = 0$, $T \approx 0$) found from the measurements [Fig. 2(a)].

B. Low density regime: mobility rollover

With the high density regime better understood, focus is now given to the $n_e < 0.8 \times 10^{12}$ cm^{-2} regime, where the Hall mobility dramatically increases with decreasing density. As the density continues to decrease, however, this behavior breaks down, and the Hall mobility begins to decrease again. This is because the mobility is calculated assuming single-carrier (electron or hole) transport. At low densities, close

to the neutrality point, transport is governed by both carrier types (electron/hole puddles),[25] and the single-carrier model is no longer valid. This is manifested as a rollover in the Hall mobility, which can be modeled with two-carrier transport [Fig. 3(b)],

$$n = \frac{\left(n_e + \frac{\mu_h}{\mu_e} n_h\right)^2}{n_e - \left(\frac{\mu_h}{\mu_e}\right)^2 n_h} \mu = \mu_e \frac{n_e - \left(\frac{\mu_h}{\mu_e}\right)^2 n_h}{n_e + \frac{\mu_e}{\mu_h} n_h}, \tag{7}$$

and a puddle density that is distributed in a Gaussian fashion on the graphene surface,

$$n_{e,h} = \int_0^\infty \int_{-\infty}^\infty \frac{1}{t\sqrt{\pi}} D(E) \left(1 + \exp\left(\frac{E \mp E_{\rm FL}}{k_B T}\right)\right)^{-1} \times \exp\left(-\left(\frac{E_{\rm FL} - E_F}{t}\right)^2\right) dE_{\rm FL} dE. \tag{8}$$

Here, μ_e and μ_h are the electron and hole mobilities, respectively; $t = \hbar v_F \sqrt{2\pi n_{pd}}$ is the characteristic energy scale of the puddle-induced surface potential fluctuation; $E_{\rm FL}$ is the local Fermi energy of a puddle; and E_F is the average Fermi energy of the system. While this rollover point does not correspond to the neutrality point [Fig. 1(b) inset], it exhibits a similar temperature dependence.[14] This is shown in Fig. 3(c), where the Hall density at the rollover point $n(\mu_{\max})$ is plotted at different temperatures. The relatively small values of $n(\mu_{\max})$ attained at low temperatures is attributed to the aforementioned electrostatic homogeneity of the graphene on SiC. Moreover, the best fit to these points using Eq. (8) and the minimum density in Eq. (7) gives a lower bound of $\nu_F \approx 1.5 \times 10^6$ m/s, a relatively high value that may be an indication of velocity renormalization due to electron–electron interactions at low densities.[26–29] While the two-carrier model explains the presence of the rollover, it does not reflect the rapid mobility increase prior to this point.

C. Full density range analysis: scatterer transparency

To further investigate the rapid mobility increase at low densities, the full density range of the Hall mobility profiles presented in Fig. 1(b) can be phenomenologically described with short-range and Coulomb scattering as the dominant scattering processes, as motivated in Sec. III A. Assuming symmetric electron and hole mobilities ($\mu_e = \mu_h$), Eq. (7) reduces to $n = (n_e + n_h)^2/(n_e - n_h)$. This expression can be put into terms of measurable quantities by utilizing the relations $n_e - n_h = C_G V_G^*/e$ and $n_e + n_h = \sqrt{(C_G V_G^*/e)^2 + n_{pd}^2}$, where $V_G^* = V_G - V_{\rm NP}$.[30] With the conductivity given by $\sigma = e\mu n = e\mu_e(n_e + n_h)$, the relationship between μ and μ_e may then be expressed in terms of n and n_{pd}:

$$\mu = \mu_e \sqrt{\frac{1 + \sqrt{1 - 4(n_{pd}/n)^2}}{2}}. \tag{9}$$

Here, n_{pd} defines the minimum value of the Hall density, $n_{\min} = 2n_{pd}$. At low temperatures, this density is found to be $n_{\min} \approx 8 \times 10^{10}$ cm^{-2} [Fig. 3(c)], giving a value of $n_{pd} \approx 4 \times 10^{10}$ cm^{-2} that can be used in Eq. (9). The electron mobility over the entire density range can then be expressed in terms of the Hall density using Matthiessen's rule $\mu_e^{-1} = \mu_C^{-1} + \mu_{\rm SR}^{-1} = \mu_C^{-1} + A_{\rm SR} n$, as outlined in Sec. III A (where the conditions $n \gg n_{pd}$ and $\mu = \mu_e$ applied). Replacing μ_e in Eq. (9) with this relation gives a final expression for the Hall mobility in terms of measurable quantities. This expression is compared to the experimental data taken at $T = 50$ K. The best fit is obtained when $\mu_C = 4750$ cm^2/Vs and $A_{\rm SR} = 0.046 \times 10^{-15}$ Vs (Fig. 4). The value of $n_{\rm SR} = (\mu_C A_{\rm SR})^{-1} = 4.6 \times 10^{12}$cm^{-2} as the onset of when short-range scattering becomes significant (i.e., $\mu_C = \mu_{\rm SR}$) is in reasonable agreement with previous experiments.[31] While Eq. (9) correctly simulates both the gradual increase in the Hall mobility with decreasing density in the $n > 0.8 \times 10^{12}$ cm^{-2} regime and the puddle-induced rollover of this mobility at low densities, it does not reproduce the sharp mobility upturn observed when $n < 0.8 \times 10^{12}$ cm^{-2}. This behavior is therefore not a consequence of Coulomb scattering, short-range scattering, or the presence of electron/hole puddles.

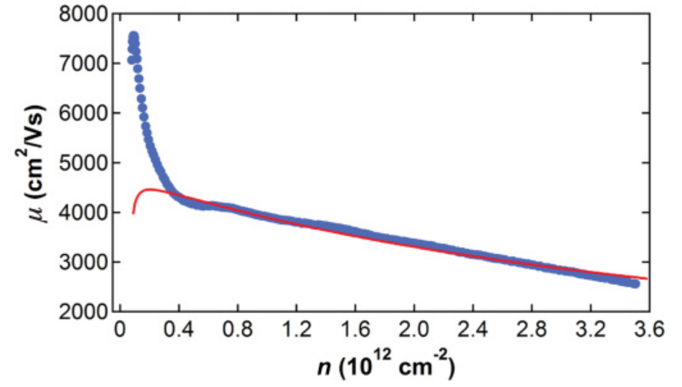

FIG. 4. (Color online) Hall mobility profile at $T = 50$ K (blue [light gray] circles) and the corresponding fit, assuming a combination of short-range and Coulomb scattering (red [dark gray] curve, Eq. (9)).

Since $k = 2\pi/\lambda = \sqrt{\pi n}$ in graphene, we suggest that decreasing n causes the carrier wavelength (λ) to increase to a point where it becomes longer than the characteristic spacing between scatterers (l_i), $\lambda > l_i \approx 1/\sqrt{n_i}$, resulting in a reduction of scattering and a corresponding increase in μ. Using $n = 0.8 \times 10^{12}$ cm^{-2} as the approximate onset of where this occurs, a carrier wavelength of $\lambda \approx 40$ nm is obtained. The intrinsic impurity density of $n_i = 1.5 \times 10^{12}$ cm^{-2} obtained from Fig. 2(a) gives an impurity spacing of $l_i \approx 8$ nm, five times less than the value of λ, in agreement with the hypothesis of scatterer transparency in the long-wavelength limit. In addition, the carrier mean free path $l_{mfp} = \sigma h/2e^2\sqrt{\pi n}$ at $n = 0.8 \times 10^{12}$ cm^{-2} is 20 nm, two times smaller than λ, also in agreement with this hypothesis.

IV. CONCLUSIONS

We provided a complete description of the Hall mobility profile of epitaxial graphene on the silicon face of 6H(0001) SiC over a wide density range. In doing so, we also provided evidence for the existence of positive charge traps in epitaxial graphene. These traps play an important role in the transport behavior exhibited by this material. Analysis of this behavior

suggests that the screening associated with these scatterers can be adequately described at high densities using RPA formalism and that the resulting transport is limited by a combination of Coulomb and short-range scattering. Furthermore, evidence of scatterer transparency is found to occur in the low density, long-wavelength regime, where an abrupt increase of Hall mobility is observed to occur.

ACKNOWLEDGMENTS

The authors thank B. Ek and J. Bucchignano for expert technical assistance. This work is supported by the Defense Advanced Research Projects Agency under Contract No. FA8650-08-C-7838 through the Carbon Electronics for Radio Frequency Applications program.

---

*dfarmer@us.ibm.com

[1] E. H. Hwang and S. Das Sarma, Phys. Rev. B **77**, 115449 (2008).
[2] S. Fratini and F. Guinea, Phys. Rev. B **77**, 195415 (2008).
[3] T. Ando, J. Phys. Soc. Jpn. **75**, 074716 (2006).
[4] E. H. Hwang, S. Adam, and S. Das Sarma, Phys. Rev. Lett. **98**, 186806 (2007).
[5] K. Nomura and A. H. MacDonald, Phys. Rev. Lett. **98**, 076602 (2007).
[6] N. M. R. Peres, J. M. B. Lopes dos Santos, and T. Stauber, Phys. Rev. B **76**, 073412 (2007).
[7] K. S. Novoselov, A. K. Geim, S. V. Morozov, D. Jiang, Y. Zhang, S. V. Dubonos, I. V. Grigorieva, and A. A. Firsov, Science **306**, 666 (2004).
[8] J.-H. Chen, C. Jang, S. Xiao, M. Ishigami, and M. S. Fuhrer, Nat. Nanotech. **3**, 206 (2008).
[9] S. Kim, J. Nah, I. Jo, D. Shahrjerdi, L. Colombo, Z. Yao, E. Tutuc, and S. K. Banerjee, Appl. Phys. Letts. **94**, 062107 (2009).
[10] K. I. Bolotin, K. J. Sikes, Z. Jiang, M. Klima, G. Fudenberg, J. Hone, and H. L. Stormer, Solid State Comm. **146**, 351 (2008).
[11] X. Du, I. Skachko, A. Barker, and E. Y. Andrei, Nat. Nanotech. **3**, 491 (2008).
[12] J.-H. Chen, W. G. Cullen, C. Jang, M. S. Fuhrer, and E. D. Williams, Phys. Rev. Lett. **102**, 236805 (2009).
[13] V. Perebeinos and Ph. Avouris, Phys. Rev. B **81**, 195442 (2010).
[14] W. Zhu, V. Perebeinos, M. Freitag, and Ph. Avouris, Phys. Rev. B **80**, 235402 (2009).
[15] C. Berger, Z. Song, T. Li, X. Li, A. Y. Ogbazghi, R. Feng, Z. Dai, A. N. Marchenkov, E. H. Conrad, P. N. First, and W. A. de Heer, J. Phys. Chem. B **108**, 19912 (2004).
[16] W. A. de Heer, C. Berger, X. Wu, M. Sprinkle, Y. Hu, M. Ruan, J. A. Stroscio, P. N. First, R. Haddon, B. Piot, C. Faugeras, M. Potemski, and J.-S. Moon, J. Phys. D Appl. Phys. **43**, 374007 (2010).
[17] X. Wu, X. Li, Z. Song, C. Berger, and W. A. de Heer, Phys. Rev. Lett. **98**, 136801 (2007).
[18] C. Dimitrakopoulos, Y.-M. Lin, A. Grill, D. B. Farmer, M. Freitag, Y. Sun, S.-J. Han, Z. Chen, K. A. Jenkins, Y. Zhu, Z. Liu, T. J. McArdle, J. A. Ott, R. Wisnieff, and Ph. Avouris, J. Vac. Sci. Technol. B **28**, 985 (2010).
[19] D. B. Farmer, H.-Y. Chiu, Y.-M. Lin, K. A. Jenkins, F. Xia, and Ph. Avouris, Nano Lett. **9**, 4474 (2009).
[20] J. Jobst, D. Waldmann, F. Speck, R. Hirner, D. K. Maude, T. Seyller, and H. B. Weber, Phys. Rev. B **81**, 195434 (2010).
[21] E. H. Hwang and S. Das Sarma, Phys. Rev. B **79**, 165404 (2009).
[22] S. Piscanec, M. Lazzeri, F. Mauri, A. C. Ferrari, and J. Robertson, Phys. Rev. Lett. **93**, 185503 (2004).
[23] V. Perebeinos, J. Tersoff, and Ph. Avouris, Phys. Rev. Lett. **94**, 086802 (2005).
[24] T. Ando, A. B. Fowler, and F. Stern, Rev. Mod. Phys. **54**, 437 (1982).
[25] J. Martin, N. Akerman, G. Ulbricht, T. Lohmann, J. H. Smet, K. von Klitzing, and A. Yacoby, Nat. Phys. **4**, 144 (2008).
[26] D. C. Elias, R. V. Gorbachev, A. S. Mayorov, S. V. Morozov, A. A. Zhukov, P. Blake, L. A. Ponomarenko, I. V. Grigorieva, K. S. Novoselov, F. Guinea, and A. K. Geim, Nat. Phys. **7**, 701 (2011).
[27] J. Gonzalez, F. Guinea, and M. A. H. Vozmediano, Nucl. Phys. B **424**, 595 (1994).
[28] J. Gonzalez, F. Guinea, and M. A. H. Vozmediano, Phys. Rev. B **59**, R2474 (1999).
[29] C.-H. Park, F. Giustino, C. D. Spataru, M. L. Cohen, and S. G. Louie, Nano Lett. **9**, 4234 (2009).
[30] I. Meric, M. Y. Han, A. F. Young, B. Ozyilmaz, P. Kim, and K. L. Shepard, Nat. Nanotech. **3**, 654 (2008).
[31] Y.-W. Tan, Y. Zhang, K. Bolotin, Y. Zhao, S. Adam, E. H. Hwang, S. Das Sarma, H. L. Stormer, and P. Kim, Phys. Rev. Lett. **99**, 246803 (2007).